# Self-trapping of polarons with off-diagonal coupling

Jin Sun,[1] Yang Zhao,[1,*] and Wanzhen Liang[1,2]
[1]*School of Materials Science and Engineering, Nanyang Technological University, Singapore 63978, Singapore*
[2]*Department of Chemical Physics and Hefei National Laboratory for Physical Science at Microscale, University of Science and Technology of China, People's Republic of China, Hefei 230026, People's Republic of China*
(Received 10 December 2008; revised manuscript received 14 February 2009; published 16 April 2009)

A variational polaron wave function pioneered by Toyozawa is utilized to elucidate exciton-phonon correlations in a generalized Holstein Hamiltonian in the simultaneous presence of diagonal and off-diagonal exciton-phonon couplings. We show that a simple analysis of quantum entanglement between excitonic and phononic degrees of freedom allows one to effectively characterize both the small- and large-polaron regimes as well as the crossover in between.

DOI: 10.1103/PhysRevB.79.155112 PACS number(s): 71.38.Ht, 03.67.Mn

## I. INTRODUCTION

In this paper we extend a previous treatment of polaronic self-trapping transition in the framework of quantum information theory.[1] Utilizing a versatile variational wave function, the Toyozawa ansatz,[2,3] we revisit the classic problem of polaron theory in one dimension incorporating simultaneous diagonal and off-diagonal exciton-phonon couplings. The former is defined as a nontrivial dependence of the exciton site energies on lattice coordinates, and the latter, as a nontrivial dependence of the exciton transfer integral on lattice coordinates. Hamiltonians containing off-diagonal exciton-phonon coupling have not been adequately addressed in the polaron literature thanks to inherent difficulties associated with obtaining accurate solutions.[4] We have shown that for diagonal exciton-phonon coupling a simple analysis of quantum entanglement between excitonic and phononic degrees of freedom allows an effective characterization of both small- and large-polaron regimes, and the crossover in between. The effect of off-diagonal coupling for exciton-phonon entanglement, however, was not considered. Previous studies[2,5] reveal that there are two branches of self-trapping lines in the two-dimensional phase diagram spanned by the transfer integral and off-diagonal exciton-phonon coupling (i.e., the case of off-diagonal coupling only). One of the self-trapping regions occurs at the zone center and the other at the zone boundary. The latter one is especially laborious to pinpoint due to numerical difficulties encountered in a variational procedure.

Previously, we undertook a numerical implementation[6] of a method proposed by Munn and Silbey[7] to determine polaron properties in the presence of simultaneous diagonal and off-diagonal couplings. The Munn-Silbey method was essentially perturbative, with the coefficients of a canonical transformation being fixed so as to limit the secular growth with the temperature of the perturbation remaining after transformation. The Munn-Silbey method is expected to produce the best description of polaron states at low temperatures as it was formulated to cure high-temperature divergence.

Our work on the Munn-Silbey method was later followed by a variational approach motivated to overcome several limitations of the Munn-Silbey method.[5] A flexible spanning set of orthonormal eigenfunctions of the joint exciton-phonon crystal momentum is used by the Toyozawa ansatz to arrive at a variational estimate of the ground-state energy for every value of the joint crystal momentum across the entire Brillouin zone (as well as the complete set of polaron Bloch functions associated with this band). In all cases studied, we have found the variational approach based on the Toyozawa ansatz to yield polaron energy bands lower than those of the Munn-Silbey method at all crystal momenta, establishing the variational energy bands as the quantitatively superior results.

Quantum entanglement[8] plays an essential role in the burgeoning field of quantum information in that it represents the key physical resource for quantum information processing.[9] Most recently, a growing amount of attention has been devoted to analysis of quantum entanglement in many-body systems undergoing quantum phase transitions.[10] In this paper we aim to investigate the polaron from this contemporary point. The particular form of quantum entanglement we will analyze is between systems of distinct physical nature: the exciton and its phonon bath. To emphasize self-trapping in the presence of off-diagonal exciton-phonon coupling, we will refer to the bipartite quantum entanglement between the exciton and its phonon environment in the polaron problem as heteroentanglement. This situation bears resemblance to those in decoherence studies where a system under examination, e.g., a qubit, is coupled with its environmental degrees of freedom, which spoils the purity of the system state. From this point of view, the polaronic entanglement to be analyzed in this paper can be viewed as a measure of the decoherence of the excitonic (phononic) state induced by the coupling with the lattice phonons (excitons). We restrict our scope here to utilizing the exciton-phonon entanglement as a tool to probe the polaronic self-trapping in the simultaneous presence of diagonal and off-diagonal exciton-phonon interactions. We make no claims on possible realizations of the exciton-phonon entanglement as a resource for quantum computation.

The paper is structured as follows. In Sec. II, the generalized Holstein model is introduced, and a detailed description of the variational ansatz is given. In Secs. III–V, we display the phase diagram with off-diagonal coupling and study the self-trapping transition using heteroentanglement at the zone center and zone boundary, respectively. Conclusions are given in Sec. VI.

 

## II. MODEL HAMILTONIAN

The Holstein molecular crystal model describes a lattice of two-level molecules interacting with a bath of nuclear degrees of freedom:

$$\hat{H} = \sum_n \Omega_n(\mathbf{q}) a_n^\dagger a_n + \sum_{m,n}^{m\neq n} J_{mn}(\mathbf{q}) a_m^\dagger a_n + \hat{H}^{\mathrm{ph}}. \tag{1}$$

Here $a_n$ ($a_n^\dagger$) are exciton annihilation (creation) operators for the $n$th molecule, $\hat{H}^{\mathrm{ph}}$ is the bath (phonon) Hamiltonian, and $\mathbf{q}$ represents the complete set of nuclear coordinates. Exciton-phonon interactions originate from dependence of molecular frequencies $\Omega_n$ and intermolecular couplings $J_{mn}$ on nuclear coordinates $\mathbf{q}$. We adopt Hamiltonian Eq. (1) with the Einstein phonon Hamiltonian

$$\hat{H}^{\mathrm{ph}} = \sum_n \hbar\omega_0 b_n^\dagger b_n, \tag{2}$$

where $b_n^\dagger$ creates a phonon of frequency $\omega_0$ on site $n$, and we have one Einstein oscillator per molecule. Exciton-phonon interactions enter through the nuclear coordinate influence on both molecular frequencies (diagonal coupling) and intermolecular interactions (off-diagonal coupling). Expanding molecular frequencies $\Omega_n(\mathbf{q})$ to the first order in phonon coordinate $\mathbf{q}$, the first term of Eq. (1) reads

$$\sum_n \Omega_n(\mathbf{q}) a_n^\dagger a_n = \sum_n \Omega_n(\mathbf{0}) a_n^\dagger a_n + \hat{H}^{\mathrm{diag}}, \tag{3}$$

with the diagonal exciton-phonon coupling term

$$\hat{H}^{\mathrm{diag}} = g\hbar\omega_0 \sum_n a_n^\dagger a_n (b_n^\dagger + b_n), \tag{4}$$

and $g$ is a dimensionless diagonal coupling constant. Expanding intermolecular couplings $J_{mn}(\mathbf{q})$ to the first order in phonon coordinates, we write the second term of Eq. (1) as, for example,

$$\sum_{m\neq n} J_{mn}(\mathbf{q}) a_m^\dagger a_n = \sum_{m\neq n} J_{mn}(\mathbf{0}) a_m^\dagger a_n + \hat{H}^{\mathrm{o.diag}}, \tag{5}$$

with the transfer integral $J_{mn}(\mathbf{0}) = -J\delta_{n,m\pm1}$ and the off-diagonal coupling term[5–7,11]

$$\hat{H}^{\mathrm{o.diag}} = \frac{1}{2}\phi\hbar\omega_0 \sum_{nl} [a_n^\dagger a_{n+1}(b_l^\dagger + b_l)(\delta_{n+1,l} - \delta_{nl}) + a_n^\dagger a_{n-1}(b_l^\dagger + b_l)(\delta_{nl} - \delta_{n-1,l})]. \tag{6}$$

The second term of Eq. (6) is the Hermitian conjugate of the first, and we have assumed nearest-neighbor coupling of the antisymmetric type with $\phi$ as a dimensionless parameter controlling the off-diagonal coupling strength. Off-diagonal coupling may adopt various forms[5,6,12] other than the antisymmetric type [Eq. (6)], and can play important roles in determining electronic properties of solids. Equations (4) and (6), together with $\hat{H}^{\mathrm{ph}}$ and the zeroth-order intermolecular coupling term, result in the generalized Holstein Hamiltonian $\hat{H}^{\mathrm{GH}}$ (the original Holstein Hamiltonian contains diagonal coupling only) (Ref. 13):

$$\hat{H}^{\mathrm{GH}} = \sum_n \Omega_n(\mathbf{0}) a_n^\dagger a_n + \hat{H}^{\mathrm{diag}} + \sum_{mn}^{m\neq n} J_{mn}(\mathbf{0}) a_m^\dagger a_n + \hat{H}^{\mathrm{o.diag}} + \hat{H}^{\mathrm{ph}}. \tag{7}$$

We may partition the generalized Holstein Hamiltonian $\hat{H}^{\mathrm{GH}}$ into three terms, namely, the exciton Hamiltonian $\hat{H}^{\mathrm{ex}}$, the phonon Hamiltonian $\hat{H}^{\mathrm{ph}}$, and the coupling Hamiltonian $\hat{H}^{\mathrm{cpl}}$:

$$\hat{H}^{\mathrm{GH}} \equiv \hat{H}^{\mathrm{ex}} + \hat{H}^{\mathrm{ph}} + \hat{H}^{\mathrm{cpl}}, \tag{8}$$

where

$$\hat{H}^{\mathrm{ex}} \equiv \sum_n \Omega_n(\mathbf{0}) a_n^\dagger a_n + \sum_{mn}^{m\neq n} J_{mn}(\mathbf{0}) a_m^\dagger a_n, \tag{9}$$

$$\hat{H}^{\mathrm{cpl}} \equiv \hat{H}^{\mathrm{o.diag}} + \hat{H}^{\mathrm{diag}}. \tag{10}$$

This generalized Holstein Hamiltonian with simultaneous diagonal and off-diagonal couplings to Einstein phonons has been previously[2,3,14,15] modeled by the Munn-Silbey approach and a variational wave function pioneered by Toyozawa, and most recently, a more sophisticated variational method has been used to solve this problem resulting in lower ground-state energy.[11] The variational wave function pioneered by Toyozawa was labeled as the Toyozawa ansatz in Ref. 3. The Toyozawa ansatz has been extended to include two-dimensional off-diagonal exciton-phonon coupling.[16] The variational methods employing relaxation iteration techniques[17,18] are shown to be rather efficient while remaining quantitatively accurate compared with calculations involving far more expensive computational resources.[19,20]

The Toyozawa ansatz has the form

$$|K\rangle = N^{-1} \sum_n e^{iKn} |\Lambda_n^K\rangle \sum_m \psi_{m-n}^K a_m^\dagger |0\rangle_{\mathrm{e}}. \tag{11}$$

Here $|K\rangle$ is the lowest energy polaron state with crystal momentum $K$, $|0\rangle_{\mathrm{e}}$ is the exciton vacuum state, and $|\Lambda_n^K\rangle$ are phonon wave functions centered at site $n$ containing a coherent state on each site $n_2$ with a displacement $\lambda_{n_2-n}^K$:

$$|\Lambda_n^K\rangle = \exp\left[ -\sum_{n_2} (\lambda_{n_2-n}^K b_{n_2}^\dagger - \lambda_{n_2-n}^{K*} b_{n_2}) \right] |0\rangle_{\mathrm{ph}}. \tag{12}$$

$|0\rangle_{\mathrm{ph}}$ is the phonon vacuum state, and $|\Lambda_n^K\rangle$ differs from $|\Lambda_{n'}^K\rangle$ only by a shift of $n$-$n'$ lattice constants. The parameters $\lambda_l^K$ and $\psi_l^K$ are obtained variationally. The phonon wave functions $|\Lambda_n^K\rangle$ represent a lattice distortion forming a potential well centered at $n$ and trapping the exciton with an amplitude distribution of $\psi_l^K$. Toyozawa ansatz state (11) is not normalized:

$$\langle K|K\rangle = \sum_{nm} e^{-iKn} \psi_m^K \psi_{m-n}^{K*} S_n^K, \tag{13}$$

where $S_n^K$ is the Debye-Waller factor

$$S_n^K \equiv \langle \Lambda_m^K | \Lambda_{m-n}^K \rangle = \exp\left[ N^{-1} \sum_q |\lambda_q^K|^2 (e^{iqn} - 1) \right], \tag{14}$$

and $\lambda_q^K$ are the Fourier transform of $\lambda_n^K$.

As in Ref. 1, we introduce the phonon-traced exciton density matrix $\rho_e^K$ for the state $|K\rangle$:

$$\rho_e^K \equiv \langle K|K\rangle^{-1}\mathrm{Tr}_{\mathrm{ph}}(|K\rangle\langle K|), \tag{15}$$

where $\mathrm{Tr}_{\mathrm{ph}}$ stands for tracing over the phonon degrees of freedom. To calculate $\rho_e^K$ we assume that exciton-phonon coupling leads to the formation of bands of collective exciton-phonon states, and the many-body polaron wave function for the ground-state band is given by the Toyozawa ansatz[2,3,14]

$$(\rho_e^K)_{mm'} = N^{-1}\langle K|K\rangle^{-1}\sum_{nn'} e^{iK(n'-n)}\psi_{m-n}^K\psi_{m'-n'}^{K^*}S_{n'-n}^K. \tag{16}$$

## III. PHASE DIAGRAM

Let us start by reviewing properties of the traditional Holstein polaron in the absence of off-diagonal coupling. For weak coupling, exciton-phonon correlations may extend over many lattice sites, forming a large polaron. With increasing coupling strength, the width of the correlated region diminishes until the excitation, together with its phonon cloud, is suddenly confined essentially to a single lattice site, creating a small polaron. Along the way, other polaron properties change as well, most notably the polaron effective mass growing from that of the bare exciton at weak coupling to values arbitrarily large in the strong-coupling region. The principal feature of such a phase diagram is a boundary line separating a small-polaron region from a large-polaron region; such a line is associated with the common notion of a more-or-less sharp self-trapping transition. The "sharpness" of this boundary line depends on the computational method; if variational approaches are used, the thickness of the boundary line would decrease with increasing sophistication of the trial states.[3]

Although on formal ground the self-trapping transition is expected to be smooth or analytical, it is commonplace for approximate treatments such as ours to encounter discontinuities where polaron structure changes in too complex a fashion to be represented accurately within the scope of the computational method. While such discontinuities must be understood to be artifacts of an insufficiently flexible method, they also serve as convenient "markers" identifying the location of significant feature on the phase diagram and thus have at least conceptual utility. The nature of this nonanalyticity is such that within the indicated regions there exists a function $K^*(J,g,\phi)$, different for each calculation method, identifying the location of a cusp in the dependence of the variational energy on $K$, i.e., at fixed $J$, $g$, and $\phi$

$$\left.\frac{\partial E^K}{\partial K}\right|_{K\to K^{*+}} \neq \left.\frac{\partial E^K}{\partial K}\right|_{K\to K^{*-}}. \tag{17}$$

If such a $K^*(J,g,\phi)$ exists, the minimum-energy states at small $K(|K|<K^*)$ are large-polaron-like and the minimum-energy states at high $K(|K|>K^*)$ are small-polaron-like while the two classes of relative minima coexist for $K^*$. The traditional self-trapping transition associated with the notion of a discrete jump in the polaron effective mass corresponds to the limit $K^*\to 0$, i.e., to the point at which the large-polaron region $K\in(-K^*,+K^*)$ is squeezed out of existence. The set of points satisfying the condition $K^*(J,g,\phi)=0$ thus constitutes the traditional "self-trapping line," which corresponds to the strong-coupling edge of the $K$-dependent transition region associated with the computational method.

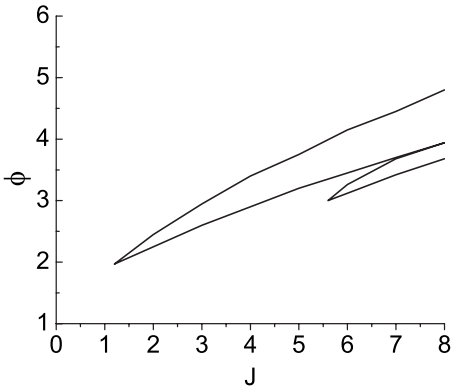


FIG. 1. Phase diagram on the $J$-$\phi$ plane for the Toyozawa ansatz. The two tongue-shaped areas correspond to the self-trapping discontinuity near the Brillouin-zone center (upper tongue) and near the Brillouin-zone boundary (lower tongue), respectively.

Our aim is to first examine the effect of off-diagonal coupling in the absence of diagonal coupling ($g=0$), and focus on the interplay between exciton transfer integral $J$ and off-diagonal coupling $\phi$. Although off-diagonal exciton-phonon coupling is a form of exciton-phonon interactions that supports polaron formation, it is also a transport mechanism and competes with diagonal coupling both by promoting transport and by driving the exciton-lattice correlations toward dimeric structures rather than the site-localized structures preferred by diagonal coupling. On the other hand, although off-diagonal coupling is a transport mechanism, it also competes with direct phonon-free exciton transfers since the lattice distortions inherent in phonon-assisted transfers inhibit direct transfers.

It is convenient to use the device of a phase diagram, as the one shown in Fig. 1, to organize our discussion. The qualitative characteristics of this familiar self-trapping transition, as described earlier for diagonal coupling, apply as well to our treatment of off-diagonal coupling. Figure 1 depicts the $J$-$\phi$ phase diagram for zero diagonal coupling strength $g=0$. Two narrow tongue-shaped regions exist dividing the plane into two more-or-less distinct sections: a strong off-diagonal coupling region occupying the upper portion of the diagram and a weak off-diagonal coupling region lying below. We find a discrete transition, which occurs in the vicinity of the Brillouin-zone center, bearing some resemblance to the more familiar diagonal coupling phenomenon; however, we also find a discrete transition occurring in the vicinity of the zone edge. Moreover, whereas the usual conception of self-trapping focuses on dramatic changes that occur at the Brillouin-zone center, leading to the notion of a sharp transition, we find the discrete transition in both the inner and outer zones to be relatively broad. In next section, we will discuss the self-trapping near the Brillouin-zone center. We delay the discussion of the zone-boundary self-trapping to Sec. V.

## IV. SELF-TRAPPING AT THE ZONE CENTER

We first consider the state of zero crystal momentum $K=0$, for which heteroentanglement between the two species in the Holstein Hamiltonian, the exciton, and the phonons, as measured by the linearized von Neumann entropy, has the form

$$E(\rho_e^{K=0}) \equiv 1 - \mathrm{Tr}_e[(\rho_e^{K=0})^2]. \tag{18}$$

Let $\hat{\rho}$ denote a density-matrix operator. Then Eq. (18) is a linearized version of the von Neumann entropy $S(\hat{\rho}) = -\mathrm{Tr}(\hat{\rho}\ln\hat{\rho})$; it shares with this latter quantity the properties: (i) $E=0 \Leftrightarrow \hat{\rho}=\hat{\rho}^2$, i.e., $\hat{\rho}$ is a pure state; (ii) $E_{\max}=1-1/D=E(\mathbf{I}/D)$, i.e., the linear entropy is at its maximum for the totally mixed state $\mathbf{I}/D$, where $D$ is the dimension of the space, and $\mathbf{I}$ is the identity matrix. Linear entropy (18) has a close relation with the so-called two-Renyi entropy,[21] and for qubits, the linear and von Neumann entropy are, conveniently, monotonic functions of each other.

In order to investigate the nature of the large- and small-polaron states, we turn to the point $(J,g,\phi)=(5,0,3.5)$. This point falls within the self-trapping area, where two distinct classes of convergent solutions to the self-consistency equations exist for $K=0$. The polaron structure of the two zone-center states corresponding to the convergent solutions is illustrated by the exciton amplitudes and the phonon displacements in Fig. 2. The solid lines are iterative results obtained when the point $(J,g,\phi)=(5,0,3.5)$ is approached from the upper portion of the phase diagram while the dashed lines from the lower portion. Consequently, the solid lines show the polaron structure typical of the upper portion of the $J$-$\phi$ plane, where off-diagonal exciton-phonon coupling is relatively strong, and the dashed lines show the polaron structure typical of the lower portion of the phase diagram, where the coupling strength $\phi$ is small. As seen in Fig. 2, the strong-coupling polaron state (solid lines) are characterized by a larger phonon displacement $\lambda_n^{\kappa}$ and a slightly more localized exciton amplitude $\psi_n^{\kappa}$ than those of the weak-coupling polaron state (dashed lines), respectively. The findings are consistent with the traditional notion of small and large polarons. The size of the polarons represented by the two solutions in Fig. 2 do not differ markedly although upon close observation the exciton and phonon amplitudes of the small-polaron state do decay somewhat more rapidly than those of the large-polaron state. A feature more characteristic of the difference between the large- and small-polaron states in the presence of off-diagonal coupling is the fact that amplitudes in the small-polaron state are characterized by more or stronger alternation of sign than found in the large-polaron state. Although these alternations are ultimately due to the antisymmetric nature of the off-diagonal coupling used in this paper, their greater prominence on the strong-coupling side of the zone-center transition in the $J$-$\phi$ plane is consistent with the more compact exciton-phonon correlations typical of small polarons.

The upper panel of Fig. 3 displays the heteroentanglement between the exciton and the phonons for $g=0$. In the $(J,\phi)$ parameter space, we first calculate the zone-center linear entanglement using convergent solutions which are obtained

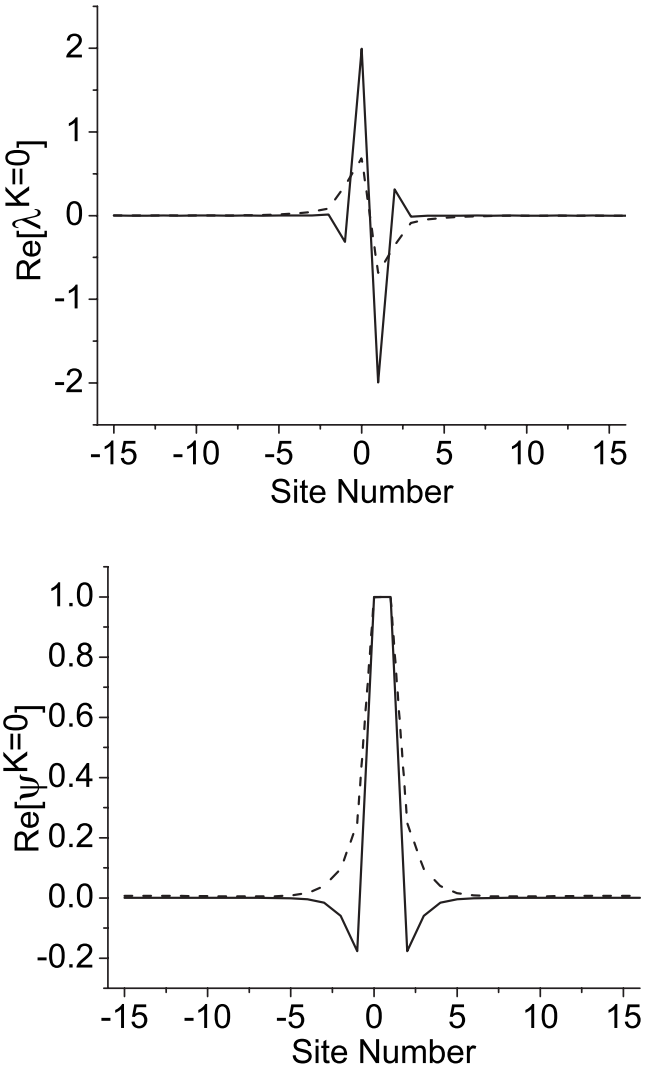


FIG. 2. Two types of convergent solution for $\mathrm{Re}[\lambda_{n=1}^{K=0}]$ (upper panel) and $\mathrm{Re}[\psi_{n=1}^{K=0}]$ (lower panel). $(J,g,\phi)=(5,0,3.5)$. The solid (dashed) line is obtained when this point is approached from the strong (weak) coupling regime, or when iteration initialization is refurbished from variational parameters bearing the strong (weak) coupling characteristics.

with iteration initializations done in the weak-coupling region (therefore, initialized states in the iteration procedure bear the large-polaron signature). As discussed earlier in Sec. III, the convergent solutions will eventually have small-polaron characteristics for all crystal momenta if the off-diagonal coupling strength exceeds a certain threshold, and the zero-momentum state is the last one to go from large to small polaron if the iteration is initialized by variational parameters with large-polaron characteristics. For zero crystal momentum, the entanglement dependence on the exciton tunneling $J$ and off-diagonal coupling $\phi$ reveals an abrupt change at some critical combinations of $J$ and $\phi$. As shown in the upper panel of Fig. 3, an entanglement bluff similar to the case of diagonal coupling only[1] is found. On the cliff plateau, the entanglement approaches its maximum value $1-N^{-1}$; on the other side of the cliff edge, the exciton-phonon heteroentanglement falls off rapidly to zero with increasing $J$ or decreasing $\phi$.

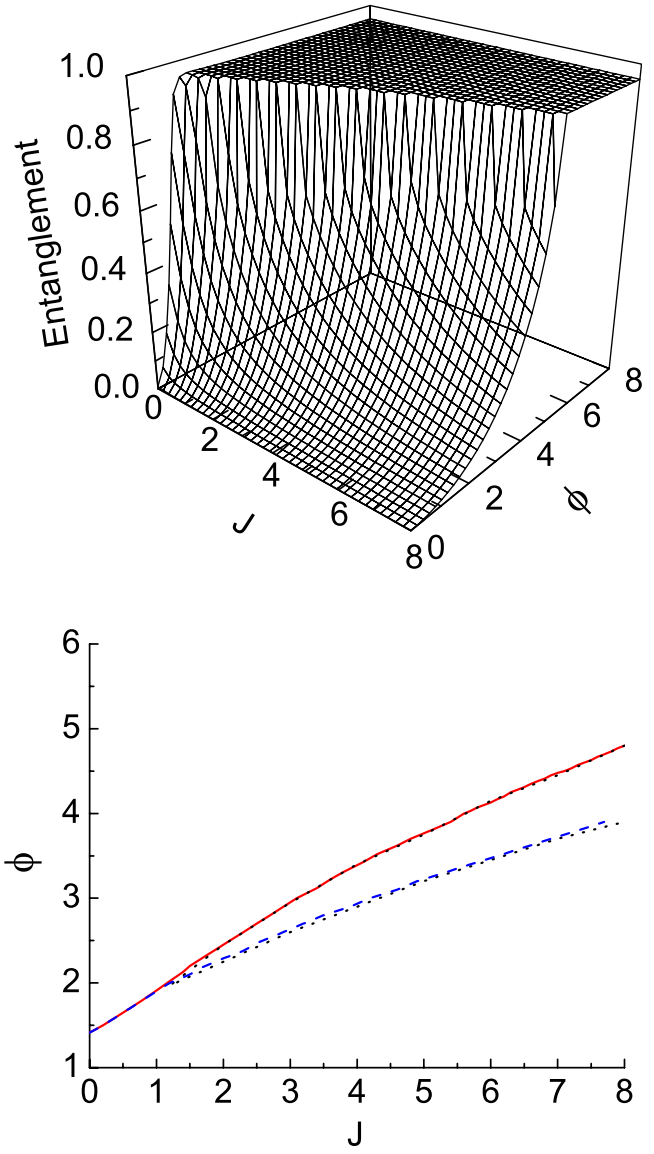


FIG. 3. (Color online) Heteroentanglement between the exciton and the phonons as measured by the linear entropy with $g=0$ is displayed in the upper panel for the entire $J$-$\phi$ phase diagram. The entanglement is calculated for the state with zero crystal momentum $K=0$. The solid and dashed lines in the lower panel are the projections of the entanglement onto the $J$-$\phi$ plane calculated from two types of convergent solution to the self-consistency equations. The solid (dashed) line is obtained from a large-polaron (small-polaron) initialization. The dotted lines depict the discontinuity tongue at the Brillouin-zone center.

When $g=0$, off-diagonal coupling competes with direct phonon-free exciton transfer integral $J$ since the lattice distortions inherent in phonon-assisted transfers inhibit direct transfers. For a given transfer integral $J$, as the off-diagonal coupling strength $\phi$ is raised, the exciton-phonon entanglement will experience a sudden increase, which coincides with the self-trapping transition. The solid line in the lower panel of Fig. 3 is the projection of the cliff edge in the upper panel onto the $J$-$\phi$ plane, which corresponds to the upper boundary of the $K=0$ discontinuity tongue in Fig. 1. It is concluded that the small polaron with strong off-diagonal coupling is a maximally entangled exciton-phonon entity while the large polaron with weak off-diagonal coupling has much-reduced exciton-phonon heteroentanglement. The entanglement between the exciton and the phonons is therefore a good measure of large and small polarons, and the transition in between.

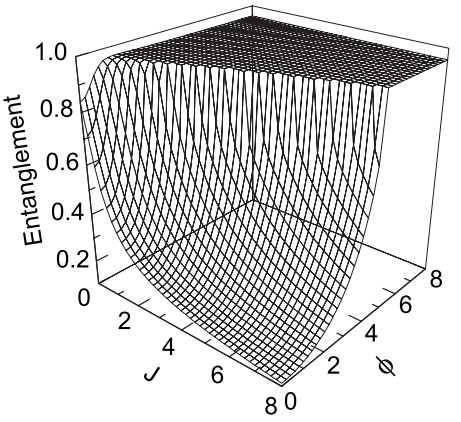


FIG. 4. Heteroentanglement between the exciton and the phonons as measured by the linear entropy with $g=1$ is displayed for the entire $J$-$\phi$ phase diagram. The entanglement is calculated for the state with zero crystal momentum $K=0$.

As shown in Fig. 2, two distinct types of convergent solutions to the self-consistency equations coexist with the tongue-shaped region in the $J$-$\phi$ phase diagram in Fig. 1. Initializing the iteration procedure with variational parameters associated with small polaron, such as the solid lines in Fig. 2, a second set of the exciton-phonon entanglement in the $(J,\phi)$ parameter space can be obtained resulting in a slightly different location of the cliff edge. The projection of the new cliff edge onto the $J$-$\phi$ plane is shown as the dashed line in the lower panel of Fig. 3. For $J<J_c=1.2$, the solid and dashed lines coincide; but as $J$ is increased beyond 1.2, the dashed line follows the lower boundary of the $K=0$ discontinuity tongue in Fig. 1. As a result, the projection lines of the entanglement cliff edges obtained by the two differing iteration initializations reproduce the tongue-shaped discontinuity boundaries in Fig. 1. Moreover, for $J<J_c=1.2$, while the discontinuity tongue no longer exists in Fig. 1, the entanglement edge is still sharp enough to leave us a clear-cut projection on the $J$-$\phi$ plane all the way to $J=0$.

In the presence of simultaneous diagonal and off-diagonal couplings, exciton-phonon heteroentanglement as a function of $J$ and $\phi$ takes a slightly different shape. Shown in Fig. 4 is the heteroentanglement as a function of $J$ and $\phi$ calculated for $g=1$ with iteration initialization done in the weak-coupling region. Compared with the upper panel of Fig. 3 ($g=0$), change in entanglement as a function of $\phi$ is less abrupt for small $J$. In the large-polaron region, heteroentanglement reaches a nonzero minimum even when $\phi=0$ due to the presence of a finite strength of diagonal coupling. Similar entanglement calculations can be repeated for iteration initialization furnished in the strong-coupling region. Consequently, projection of the heteroentanglement cliff edges onto the $J$-$\phi$ plane can also be carried out for $g=1$ and higher values of diagonal coupling. Combining all projec-

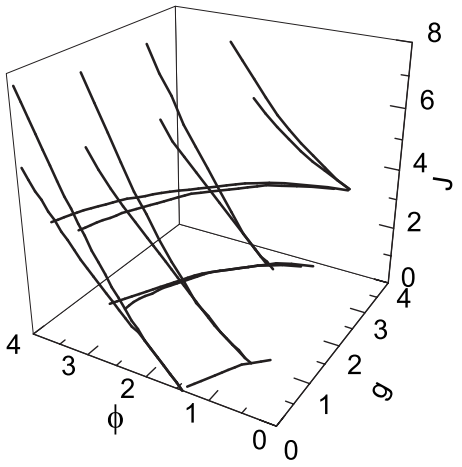


FIG. 5. Projection of heteroentanglement cliff edges onto the $J$-$\phi$ plane for four values of $g$: $g=0$, 1, 2, and 3. Heteroentanglement between the exciton and the phonons is measured using the linear entropy. Also shown is projection of heteroentanglement cliff edges onto the $g$-$\phi$ plane for four values of $J$: $J=0$, 2, and 4.

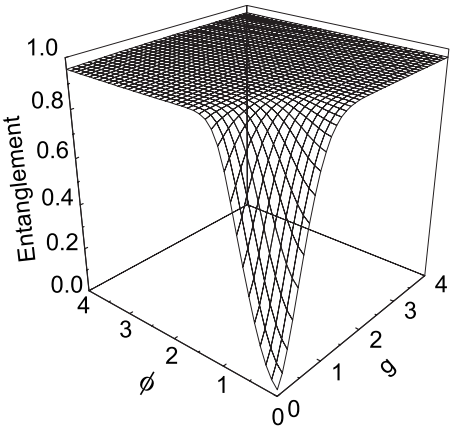


FIG. 6. Heteroentanglement between the exciton and the phonons as measured by the linear entropy with $J=0$ is displayed for the entire $g$-$\phi$ phase diagram. The entanglement is calculated for the state with zero crystal momentum $K=0$.

tions in the three-dimensional parameter space spanned by $J$, $g$, and $\phi$ reveals a three-dimensional phase diagram for the Toyozawa ansatz, which is displayed in Fig. 5. Altogether, the exciton-phonon heteroentanglement for four values of diagonal coupling, $g=0$, 1, 2, and 3, is calculated and projected onto the $J$-$\phi$ plane. For each $g$, two types of iteration initialization are furnished to the variational procedure. We find that the presence of $g$ facilitates the transition from large polaron to small polaron such that self-trapping happens for a smaller $\phi$.

Next we confine our attention to the interplay between $g$ and $\phi$ with the transfer integral in the absence of the transfer integral ($J=0$). The case of zero $J$ and nonzero $\phi$, however, is not very realistic as $\phi$ comes out of the first-order derivative of $J$ with respect to the phonon coordinate. One close realization of the limit of zero $J$ and nonzero $\phi$ would be molecular crystals with small transfer integrals where, upon involvements of certain phonon modes, such as the librational modes, the electronic overlap integrals between adjacent molecules can be greatly enhanced. Figure 6 shows the entanglement between the exciton and the phonons as a function of diagonal and off-diagonal couplings. An entanglement cliff is found with the entanglement approaching $1-N^{-1}$ on the cliff plateau, and dropping precipitously to zero on the other side of the cliff. When $J=0$ and $\phi=0$, the exact solution to the Holstein Hamiltonian includes a displaced oscillator with the phonon displacement localized on the site where the exciton resides:

$$|\Psi\rangle = \sum_n \psi_n a_n^\dagger \exp[-g(b_n^\dagger - b_n)]|0\rangle_{\text{ex-ph}}. \tag{19}$$

Then the phonon-traced exciton density matrix has the form

$$(\rho_e^K)_{m,m'} = N^{-1} \exp[-g^2(1-\delta_{m,m'})]. \tag{20}$$

If $g$ is large, the off-diagonal elements of the density matrix vanish so that the entanglement between the exciton and the phonons approaches $1-N^{-1}$; if $g=0$, a phonon vacuum state leads to zero entanglement and that $(\rho_e^K)_{m,m'}=N^{-1}$, and the density matrix satisfies the property $\rho=\rho^2$. As $g$ is reduced to zero, so is the entanglement between the exciton and the phonons. The entanglement cliff edge in Fig. 6 can be projected onto the $g$-$\phi$ plane, and the projection is sketched as a line at the bottom of Fig. 5. If $J$ is increased, such a line projection onto the $g$-$\phi$ plane will be split into two intersecting lines, between which two convergent solutions to the self-consistency equations are found. This has been demonstrated clearly in Fig. 5, where two additional projection lines onto the $g$-$\phi$ plane are shown for $J=2$ and 4.

## V. SELF-TRAPPING AT THE ZONE BOUNDARY

In this section, we consider the state of crystal momentum $K=\pi$. In the absence of diagonal coupling, the phase diagram spanned by transfer integral $J$ and off-diagonal coupling $\phi$ has a second self-trapping region near the Brillouin-zone boundary, shown by the smaller, much narrower tongue-shaped region in Fig. 1. The zone-edge transition is, in many ways, similar to the zone center one except that $K^*$, defined by Eq. (17), will now be pushed toward the Brillouin-zone edge (instead of $K=0$) with increasing $\phi$. In the large-polaron region below the transition in the $J$-$\phi$ phase diagram, a plane-wave component dominates the phonon amplitudes while, after crossing over into the small-polaron region, this plane-wave component is absent.[5] The zone-edge transition can be viewed as a binding or unbinding of the free-phonon component. It is suggested that the zone-edge state on the weak-coupling side of this transition is not simply a large-polaron state but a mixture of large polarons essentially at rest and "unbound" free phonons.

Despite many interesting phenomena associated with the zone-edge transition, the discontinuity region near $K=\pi$ is much more difficult to probe due to poor numerical convergence encountered at the zone boundary in the iterative procedure. This gives us more reasons to apply our new method of using exciton-phonon entanglement as a measure to determine the large and small polarons, and the transition in be-

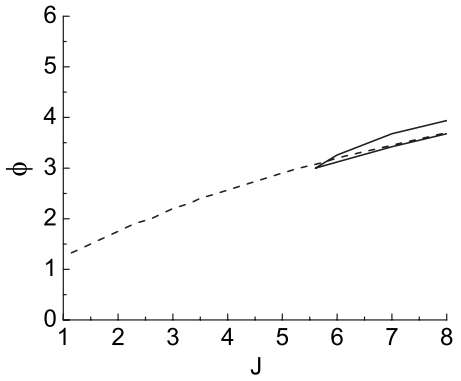


FIG. 7. A thin tongue-shaped discontinuity region near the Brillouin-zone boundary in the absence of diagonal coupling (solid line) and the projection of the entanglement cliff edge onto the $J$-$\phi$ plane calculated for crystal momentum $K=\pi$ $g=0$(dashed line).

tween. Similar to Eq. (18), heteroentanglement between the two species in the Holstein Hamiltonian, the exciton, and the phonons, as measure by the linearized von Neumann entropy, has the form

$$E(\rho_e^{K=\pi}) \equiv 1 - \mathrm{Tr}_e[(\rho_e^{K=\pi})^2]. \tag{21}$$

Similar to the $K=0$ case, we also obtain an entanglement cliff from applying the above expression: Eq. (21) approaches a maximum value $1-N^{-1}$ on the cliff plateau, and falls off rapidly to zero on the other side of cliff edge. However, contrary to the $K=0$ case, little difference in entanglement edge positions is found between the two convergent solutions derived from different types of iteration initializations. Projection of the entanglement cliff edge onto $J$-$\phi$ plane, a sharp boundary between the small and large entanglement regions, is shown in Fig. 7 (dashed line) for crystal momentum $K=\pi$. The projection line goes right through the discontinuity tongue (solid line) near the Brillouin-zone boundary. In addition, the projection line also unambiguously divides the $J$-$\phi$ phase diagram into the large- and small-polaron state regions. As one travels vertically upward in the $J$-$\phi$ phase diagram, entanglement between the exciton and the phonons increases, and at the same time, the polaronic structure morphs from large polaron to small polaron. By analyzing the heteroentanglement, we can distinguish the small- and large-polaron states near the zone edge ($K=\pi$), and make sure where the transition will take place even if numerical difficulties prevent the discontinuity tongues from being determined precisely near the Brillouin edge.

## VI. CONCLUSION

Three quarters of a century have passed since the concept of polaronic self-trapping was first conceived by Landau,[4,22–27] and yet questions linger on some fundamental properties of polaron Hamiltonians. In this paper, we investigate the polaron problem with off-diagonal exciton-phonon coupling using the quantum entanglement between the excitons and the phonons as a probing tool. By considering the off-diagonal coupling in Holstein Hamiltonian, we get the heteroentanglement between the exciton and the phonons, and study the dependence of entanglement on diagonal or off-diagonal coupling and exciton transfer integral. We find the heteroentanglement is a good measure of large and small polarons, and the transition in between: the small polaron is a maximally entangled exciton-phonon entity while the large polaron has much-reduced exciton-phonon heteroentanglement. With off-diagonal coupling, self-trapping focuses on dramatic changes occurring at both vicinities near the Brillouin-zone center and edge. Since entanglement can embody the property of polaron, by observing the abrupt change in exciton-phonon entanglement, we can investigate the self-trapping more clearly, especially near the Brillouin boundary which cannot be solved with precision previously.

## ACKNOWLEDGMENT

Support from the Singapore Ministry of Education through the Academic Research Fund (Tier 2) under Project No. T207B1214 is gratefully acknowledged.

*yzhao@ntu.edu.sg

[1] Y. Zhao, P. Zanardi, and G. H. Chen, Phys. Rev. B **70**, 195113 (2004).
[2] Y. Zhao, Ph.D. thesis, University of California, 1994.
[3] Y. Zhao, D. W. Brown, and K. Lindenberg, J. Chem. Phys. **107**, 3159 (1997); D. W. Brown, K. Lindenberg, and Y. Zhao, *ibid.* **107**, 3179 (1997); Y. Zhao, D. W. Brown, and K. Lindenberg, *ibid.* **106**, 5622 (1997); A. Romero, D. W. Brown, and K. Lindenberg, *ibid.* **109**, 6540 (1998).
[4] L. D. Landau, Phys. Z. Sowjetunion **3**, 664 (1933); G. D. Mahan, *Many Particle Physics* (Plenum, New York, 1981).
[5] Y. Zhao, D. W. Brown, and K. Lindenberg, J. Chem. Phys. **106**, 2728 (1997).
[6] Y. Zhao, D. W. Brown, and K. Lindenberg, J. Chem. Phys. **100**, 2335 (1994).
[7] R. W. Munn and R. Silbey, J. Chem. Phys. **83**, 1843 (1985); **83**, 1854 (1985).
[8] M. Horodecki, P. Horodecki, and R. Horodecki, in *Quantum Information: An Introduction to Basic Concepts and Experiments*, edited by G. Alber (Springer, Berlin, 2001).
[9] For reviews, see C. H. Bennett and D. P. Di Vincenzo, Nature (London) **404**, 247 (2000); A. Steane, Rep. Prog. Phys. **61**, 117 (1998).
[10] T. J. Osborne and M. A. Nielsen, Phys. Rev. A **66**, 032110 (2002); A. Osterloh, L. Amico, G. Falci, and R. Fazio, Nature (London) **416**, 608 (2002); G. Vidal, J. I. Latorre, E. Rico, and A. Kitaev, Phys. Rev. Lett. **90**, 227902 (2003).
[11] Y. Zhao, G. Q. Li, J. Sun, and W. H. Wang, J. Chem. Phys. **129**, 124114 (2008).
[12] S. Ishihara and N. Nagaosa, Phys. Rev. B **69**, 144520 (2004).

[13] T. Holstein, Ann. Phys. (N.Y.) **8**, 325 (1959); **8**, 343 (1959).
[14] Y. Toyozawa, Prog. Theor. Phys. **26**, 29 (1961).
[15] V. M. Buinmistrov and S. I. Pekar, Sov. Phys. JETP **5**, 970 (1957).
[16] Y. Zhao, G. H. Chen, and L. Yu, J. Chem. Phys. **113**, 6502 (2000).
[17] Y. Zhao and H. N. Bertram, J. Magn. Magn. Mater. **114**, 329 (1992).
[18] Y. Zhao and H. N. Bertram, J. Appl. Phys. **77**, 6411 (1995).
[19] E. Jeckelmann and S. R. White, Phys. Rev. B **57**, 6376 (1998).
[20] J. Bonca, S. A. Trugman, and I. Batistić, Phys. Rev. B **60**, 1633 (1999).
[21] A. Renyi, *Proceedings of the Fourth Berkeley Symposium Mathematical Statistics and Probability, 1960* (University of California Press, Berkeley, 1961), Vol. 1, p. 547.
[22] S. I. Pekar, J. Phys. (Moscow) **10**, 341 (1946).
[23] K. Huang and A. Rhys, Proc. R. Soc. London, Ser. A **204**, 406 (1950).
[24] T. D. Lee, F. E. Low, and D. Pines, Phys. Rev. **90**, 297 (1953).
[25] R. P. Feynman, Phys. Rev. **97**, 660 (1955).
[26] E. I. Rashba, Opt. Spektrosk. **2**, 75–88 (1957).
[27] J. J. Markham, Rev. Mod. Phys. **31**, 956 (1959).